Biomedical Engineering Letters (2020) 10:43–61
https://doi.org/10.1007/s13534-019-00132-w

REVIEW ARTICLE

Review of functional materials for potential use as wearable infection sensors in limb prostheses

Harish Devaraj[1] · **Kean C. Aw**[1] · **Andrew J. McDaid**[1]

Received: 26 April 2019 / Revised: 30 July 2019 / Accepted: 17 September 2019 / Published online: 3 October 2019

Abstract
The fundamental goal of prosthesis is to achieve optimal levels of performance and enhance the quality of life of amputees. Socket type prostheses have been widely employed despite their known drawbacks. More recently, the advent of osseointegrated prostheses have demonstrated potential to be a better alternative to socket prosthesis eliminating most of the drawbacks of the latter. However, both socket and osseointegrated limb prostheses are prone to superficial infections during use. Infection prone skin lesions from frictional rubbing of the socket against the soft tissue are a known problem of socket type prosthesis. Osseointegration, on the other hand, results in an open wound at the implant-stump interface. The integration of infection sensors in prostheses to detect and prevent infections is proposed to enhance quality of life of amputees. Pathogenic volatiles having been identified to be a potent stimulus, this paper reviews the current techniques in the field of infection sensing, specifically focusing on identifying portable and flexible sensors with potential to be integrated into prosthesis designs. Various sensor architectures including but not limited to sensors fabricated from conducting polymers, carbon polymer composites, metal oxide semiconductors, metal organic frameworks, hydrogels and synthetic oligomers are reviewed. The challenges and their potential integration pathways that can enhance the possibilities of integrating these sensors into prosthesis designs are analysed.

Keywords Prosthesis · Amputee · Infection · Sensing · Materials

1 Introduction

Prosthetic devices date back thousands of years and they have been in use with varying levels of success since their inception [1, 2]. The advancements in the field of robotics and healthcare have revolutionized the field of prosthesis in recent years and are continuing to improve the quality of life for amputees [3–6]. The constantly increasing research interests on these prosthetic devices can be attributed to the need for further improvement of the functionality and safety of these devices.

The functionality of these devices could be measured through a measure of their everyday performance levels. The close replicability of the full range of motion (RoM) and amputee specific design with appropriate parameters such as physical dimensions and mass can be construed as a measure of the biomechanical performance of the prosthetic device. Apart from mechanical functionality of prosthetic device, the second main measure of the goodness of a prosthetic is the comfort level they can provide to the amputee. This encompasses the goodness of fit and the extent of seamless integration to the residual limb of the amputee with minimal tissue damage.

The functionality improvement in prosthetics has been constantly evolving in parallel with innovative technologies. From sixteenth-century, the increasing use of mechanisms and gears have resulted in replacement of single link prosthesis [7] to a multilink prosthesis [8] and in more recent times, with the advent of information age and microelectromechanical systems (MEMS), the ability to integrate complicated controllers and sensors to the prosthetics [5, 6] has resulted in improved functionality. Furthermore, in the late twentieth-century, the advancements in 3D printing technology have enabled fabrication of numerous prosthesis designs that were deemed complex for traditional fabrication methods [9–13].

✉ Andrew J. McDaid
andrew.mcdaid@auckland.ac.nz

[1] Department of Mechanical Engineering, Faculty of Engineering, The University of Auckland, Auckland, New Zealand

1.1 Limb prosthesis

Socket prosthesis has been the dominant form of prosthesis since the early days of prosthetics [1, 8] and is still to date the widely prescribed form of prosthesis. With the increase in computational capabilities, socket prosthesis design has been optimized through finite element models [14, 15]. Improvements in wireless communications technology and the onset of Internet of Things have further enabled prosthetic manufacturers and researchers to embed various sensors capable of measuring prosthetic loads [16–18], the RoM/gait of the patients [19–21] and in some cases even provide sensory feedback to the patients [22]. Despite the various improvements to the socket prosthesis designs over time, studies of periodic surveys of amputees who have been prescribed socket type prosthesis [23, 24] clearly indicate that despite their long established history as a prosthetic device, they are extremely uncomfortable.

Socket based prosthesis essentially wrap around the residual limb of an amputee as schematically shown in Fig. 1a. This constant contact between the socket and the soft tissue combined with the movement-induced shearing between the socket surface and the residual limb, the load-induced changes in frictional forces on the soft tissue and slippage of socket have been commonly reported as causality for discomfort. These factors not only induce discomfort to the amputees, but have also been reported to be a contributing factor for various ailments such as but not limited to edema, skin irritation, cysts and blisters as reviewed by Lyon et al., Levy et al., and Meulenbelt et al. [25–27]. These complications when left unchecked can result in infection of the socket-tissue interface areas making use of socket prosthesis impossible until the infection is treated and the skin complication is healed.

The introduction of osseointegration process in the early 1950s and a pioneering surgical procedure of osseointegrated dental implants by Brånemark demonstrating osseointegration as a technique for rehabilitations, have led way to a far better and more functional alternative to traditional prosthetics [28]. While over 800,000 patients have undergone dental osseointegration, since 1965, with long-term success rates [29] and over 2000 published medical articles, strong basis for this surgical procedure has been laid out. Following this, more recently this surgical procedure administered for upper and lower limb amputees. A schematic of a typical osseointegrated implant is shown in Fig. 1b. With the implant being in contact directly with the bone tissue, the microcirculation of the bone around the load carrying implant provides a much stronger musculoskeletal level integration. As shown in Fig. 1b, the titanium implant acts as a direct extension of the residual bone and would thus enable far greater mechanical loading with minimal discomfort for the patient. This transcutaneous implant architecture has demonstrated far greater comfort levels and patient satisfaction (95%) over traditional socket type prostheses [30, 31]. In a study carried out by Meent et al. [32] on the walking ability of amputees with prosthetics, the patients with osseointegrated prosthesis were capable of walking 44% faster and 27% longer than patients with socketed prosthetics. Despite being a newer medical procedure, the average osseointegrated prosthesis medical cost, according to Haggstrom et al. [33] is approximately €500/year lesser than socket prostheses.

Osseointegrated prosthesis having been demonstrated to be far superior to that of socketed prostheses, is not free of drawbacks. The transcutaneous architecture of the prosthesis demands a surgical procedure for the insertion of the titanium implant into the residual bone. This results in an open wound at the implant-stump interface. While successful healing of this wound can result in a complete and strong osseointegration, any incomplete healing of this wound might result in repeat surgery and in some cases even complete removal of the titanium structure. Clinical reviews conducted following osseointegration process clearly indicate

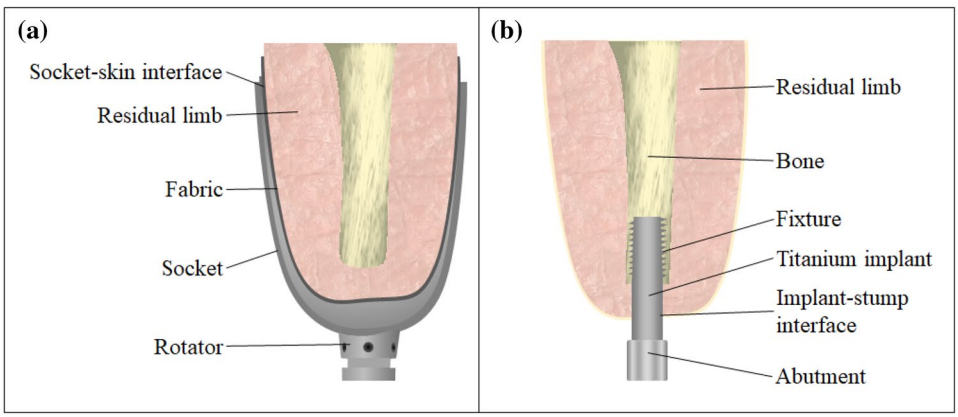

Fig. 1 Representative cut-section showing **a** socket type prosthesis and **b** osseointegrated implants

the main reason behind unsuccessful osseointegration as tabulated in Table 1.

The main complication associated with osseointegrated implants was clearly infections (both superficial and deep infections). Deep implant infections are typically a result of nosocomial (hospital environment related) pathogens that can attach on to the implant or the open wound during surgical procedure. Superficial infections however can be picked up by the patient both while in the hospital and from external sources following the surgical procedure. The superficial infections when left unchecked can spread and manifest as deep implant infections. Branemark et al. [35] in his recent study reported that among 11 patients with deep implant infections, the infection-impaired bone-implant bonding resulted in an early loosening of the implant. While non-infectious complications due to improper loading and insufficient rehabilitation associated with this relatively newer surgical procedure are fairly low (< 10%), the primary cause of repeat surgeries and implant removal could be associated to infectious complications.

1.2 Infectious complications

Infection related complications being a commonplace in both the traditional socket prostheses and the more recent osseointegrated prosthesis, it becomes critical to address this issue to ensure these prostheses are more robust, reliable and safe. The pathogens (mostly bacteria and in some cases viruses) are present even in cleaner and hygienic hospitals in developed countries [37]. It was identified that most nosocomial bacteria and viruses can survive on inactive surfaces for months together and can be a source of transmission unless the surface is regularly disinfected [38]. A complete and thorough disinfection is not possible and furthermore, the threat of antimicrobial resistant bacteria [39] further complicates this issue. Biofilm formation on implants have also been identified to be the most devastating complication and the review by Gbejuade et al., clearly outlines the formation of biofilms and their effect on a successful joint arthroplasty [40]. Among 39 patients studied, it was identified that over 40% of the patients showed signs of *Staphylococcus aureus* (*S. aureus*) infections with 25% of the patients showing signs of *Coagulase-Negative Staphylococci* infections. The remaining patients exhibited signs of various *Streptococci* strains, *Enterococcus faecalis*, *Escherichia coli* (*E. coli*) and *Pseudomonas aeruginosa* infections at the implant-stump interface with several patients were identified to be infected with more than one bacterial species [40]. Superficial infections, if identified in early stages can be easily cured, but deep implant infections if present poses a more serious threat.

The implant during the surgical procedure is not completely isolated from any air-borne or contact-transferred pathogenic contaminants. Their instantaneous adhesion onto the titanium surface has been identified as the most critical step for introducing pathogens into the soft tissue of the amputee [41]. With the release of such findings, novel self-sterilizing coatings such as those created by Ohko et al. [42] and antibacterial coatings [43], especially those that specifically prevent *S. aureus* adhesion to implants [44] have been developed and implemented. Furthermore, to deter deep implant infections, antibiotic pellets are also placed before the wound is sutured during the surgical procedure. After released from surgical care, any presence of infection and lack of detection of early stage infections can lead to propagation of infection into the implant-stump interface. Patient carelessness and oversight on medication could be attributed as a major source of superficial infections and further complications resulting from these infections.

From sensors that can accurately monitor the pressure levels exerted on the prosthesis to sensors that can monitor the structural health, the prosthesis industry would greatly benefit from a novel sensor that can accurately identify the early stage infections irrespective of the species of pathogen present. Detection of pathogen is however not a simplistic procedure. Traditional approach for infection diagnosis is through periodic physical swab sample collection. The patient is required to visit the hospital to provide a cotton swab sample from the open wound. This swab sample is then cultured on a nutrient medium which might take anywhere between 24 and 48 h depending upon the potency of pathogens present. As the sample collection and culture preparation locations are usually not at the same place, the contamination of swab sample during the transit or handling process can result in false positives. This process has already been deemed too slow and ineffective in most cases when the

Table 1 Complications from follow up studies on patients with osseointegrated prosthesis

Clinical review	Referenced articles	Average skin infections/complications rate (%)	Implant loosening/fracture rate	Average repeat surgeries rate	Average implant removal rate
Meent et al.	[32]	36	–	–	–
Branemark et al.	[34, 35]	55	4%	–	8%
Aschoff et al.	[30, 31, 36]	46	2%/7%	60%	9%

culture's nutrient medium may not support multiplication of certain bacterial species. Hence, alternative approaches have also been established such as use of enzyme immunoassays [45], polymerase chain reactions [46] and ligase chain reaction assays [47]. While these approaches have been demonstrated to be more effective in diagnosing bacterial presence, the number of steps involved in identifying the strain such as selection of primer sequences for effective amplification of the sampled DNA and in assay preparation increases the complexity of the process. Any wrong selection of the primer sequence or the contamination introduction can again result in false positives. Even when carefully controlled, these approaches still make use of chemical assays. The use of such assays makes it extremely difficult for integration into prosthesis designs. Hence, an alternative approach to detecting bacterial presence is needed.

2 Infection sensing through olfaction

As ways of determining wound infections, albeit only the late stages of infections, the Greek and the Chinese, as early as 2000 BCE, have used olfaction or 'smell'. An infected wound smells vastly different (in most cases pungent smelling) than that of a healthy wound which was used as an indicator of infection presence [48]. Pathogens, being a basic lifeform, metabolize nutrients for survival. The nutrient metabolism results in the release of metabolites from pathogens. These metabolites are in essence volatile organic compounds (VOCs) that emanate from the wound surface. This ancient method of infection diagnosis has been long discarded, as this approach is only suitable for later stages of infections only when significant number of bacterial colony forming units (CFUs) were present. Recently the advancement in gas chromatography and mass spectrometry (GC/MS) techniques have been demonstrated to be capable of sampling broad range of volatiles released from bacterial colonies with high sensitivity and accuracy.

Increasing interest in exploiting the volatile analysis technique to detect pathogen presence is evident from increasing number of research articles published in the field of breath research focussing on capturing and analysing breath volatiles [49–51]. Zhu et al. [51] have demonstrated the ability of volatile analysis technique to distinguish *Pseudomonas aeruginosa* infection from *S. aureus* infection in mice models from sampling their exhaled breath. While these research articles demonstrate the viability of using volatiles to identify pathogen presence, the use of solid phase micro extraction for sampling volatiles restricts the range and detection limits. Furthermore, the forced induction of volatiles into the sampling instrument for analysis make these approaches unsuitable for sampling volatiles directly from open-wounds. In these lines, our recent work makes use of a more recently developed sampling technique called stir-bar sorptive extraction (SBSE) [52]. This technique allows sampling of volatiles released from a static substrate with minimal need for forced induction. The large sorptive volume of the sampling media allowed identification of the chemical composition of the volatiles released from *E. coli*. Over 145 different volatile compounds with trace elements down to picomolar concentrations were identified [52]. Further work on four different bacterial species paved way for the development of a database of bacterial volatiles, demonstrating the ability to use the unique volatile biomarkers as an indicator for the presence of particular species of bacteria. With volatile biomarkers having been identified and established in being capable of providing information on not only the species of the pathogen but differentiate between strains of a particular pathogenic species [50], the potential for using these volatile biomarkers as a sensing stimulus is promising.

3 Volatile biomarker sensing

Volatile biomarkers, while being a potent stimulus for signalling infection presence and identifying infection type (both pathogenic species and strain), the research so far on sampling and analysing these volatiles has been reliant upon highly expensive and bulky GC/MS instruments that would take up the size of a small sized car. Though researches in developing lab-on-chip MS [53] and MEMS GC columns [54] have been underway, they have been limited to liquid phase separation with a noticeable loss of resolution due to miniaturization. The results from a MS instrument as detailed in [52] still demand further data analysis, to identify individual fragments of the component ions and compound identification from the spectral data by matching them against an existing database with specific software. To extract the resolution and accuracy of such a bulky setup and automating the compound identification process towards integrating them into a prosthetic device is far from achievable at present. Hence, alternative means of identifying these volatiles is necessary. The following sections analyse the suitability of potential volatiles/gas sensing functional materials that demonstrate potential for miniaturization and integration into future prosthetic designs. While a gamut of gas sensing techniques are available, owing to the target application's demands, this review only focusses on fundamental sensing techniques, materials and processes used that would allow potential integration into future prosthetic designs. In these lines, only sensing techniques that can be realized in the form of flexible/elastic architecture with intention of embedding the potential sensing architecture into a fabric/elastic bandage that wraps around the osseointegrated prosthesis-residual limb interface for detecting infection are reviewed.

3.1 Electronic noses

The term electronic nose or simply E-nose, coined in the 1980s, represents an instrument that contains a heterogeneous array of electrochemical sensors with partial specificity and a pattern recognition system [55]. Electrochemical gas sensors produce a change in their electrical activity (change in conductivity) upon exposure to certain gases. These gas molecules bind to the functional chemical compound (sensing material) which may be purely sorptive (surface adsorption) or a combination of adsorption with physical absorption or through chemisorption (chemical reaction induced binding). The selection of the functional material will depend on the mode of binding preferred.

Binding of target gas molecules through chemisorption is only used in applications where high selectivity is preferred which is a necessity in infection sensors. This selectivity would ensure change in electrochemical response of the functional material only in the presence of the target volatile biomarker. For instance, the presence of indole (C_8H_7N) in the wound volatiles is a positive indicator for the presence of *E. coli* infection. Any chemical capable of a strong reaction to indole would thus be an ideal functional material/sensing element in an E-nose for *E.coli* infection detection. The most sensitive reagent used in laboratory tests that reacts with dissolved indole is p-dimethylaminocinnamaldehyde [56]. However, the use of this reagent as a freestanding electrochemical sensor capable of reacting with indole in gaseous phase is not possible. Moreover, chemical reaction of such reagents with indole molecule is an irreversible reaction. Hence, any E-nose based on such chemisorption-based mechanism cannot be implemented as a reusable sensing device to detect pathogens in future prosthetic devices. Physisorption and weak chemisorption based E-noses, which typically use metal oxide semiconductors (MOx), conducting polymers (CPs) and carbon based composites are seeing a strong growth. Their sensing mechanism and their potential for use in infection sensing is analysed in the upcoming sections.

3.1.1 Metal oxide semiconductor (MOx)

This type of functional material is the most widely used sensing element in E-nose applications. It demonstrates high levels of sensitivity to various organic vapours with a fast response time. Having a simpler chemical composition as opposed to other functional materials used in E-nose applications, MOx sensors have a stable lifetime and are readily available commercially with little to no further chemical processing needed. The operating principles of metal oxide semiconductors are schematically represented as in Fig. 2a and commercially available MOx based gas sensors are shown in Fig. 2b. The metal oxides have a large band gap due to a wide space-charge region with oxygen ions surrounding the metallic core in case of an n-type MOx. The ionosorbed oxygen (O_2) restricts electron flow among the metal oxides. However, at temperatures greater than 150 °C (in some cases even higher temperatures up to 300 °C is required [57]), it becomes ionosorbed as O^-. This ionosorbed oxygen can easily combine with a reducing gas (n-type MOx—typical examples include tin oxide, zinc oxide or iron oxides) which would allow a release of free electron into the space-charge region as shown in Fig. 2a. Thus, in the presence of a reducing gas and at an operating temperature above 150 °C, the excess electrons released into the space-charge region deplete this potential barrier allowing increased conductivity. The similar process is reversed in case of p-type semiconductors usually comprising oxides of nickel or cobalt where the hole transfer occurs in presence of oxidizing gases. This increased conductivity is measured

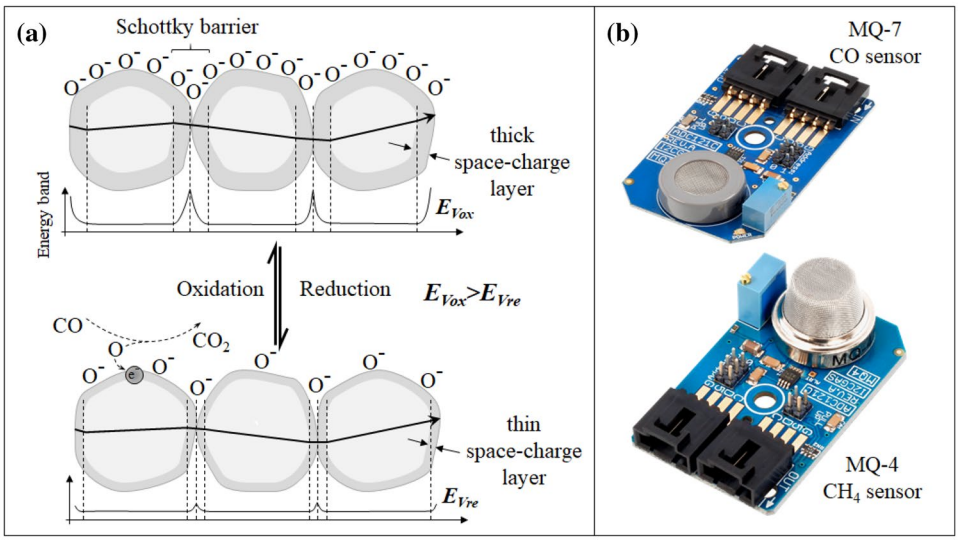

Fig. 2 **a** Schematic representation of conduction mechanism during oxidation and reduction. **b** Commercially available MOx based gas sensors

as a decrease in resistance by the accompanying electronics to read out rapid and sensitive detection of the analyte gases.

The reversible mechanism at lower temperatures allows rapid desorption of the reducing/oxidizing gases from the surface of the metal oxide semiconductors. While surface adsorption of the gases has been identified to be highly sensitive, research into further improving their sensitivity through converting bulk MOx into nanostructured particles has also been underway. Table 2 summarizes various highly sensitive MOx based gas sensors with improved selectivity, through use of catalysts or hybrid mixtures that have been published. However, owing to the extremely large

Table 2 Metal oxide semiconductor based gas sensors and their operating parameters

Sensing Gas	MOx type	Sensing temperature	Detection Limits	Response Time	References
Acetone	CdO	300	< 20 ppm	3 s	[58]
	Fe_2O_3 + Pt/Pd/RuO_2	300	0.1–20 ppm	3 s	[58]
Butane	ZnO (Al, In, Ga)	200–350	2–1000 ppm	2 min	[59]
	Ga_2O_3 + SnO_2	500–950	100 ppm	1 min	[61]
Methane	Ga_2O_3 + SnO_2	500–950	10,000 ppm	1 min	[61]
Chlorine	In_2O_3 + Fe_2O_3	250–500	0.1–5 ppm	2 min	[62]
Carbon monoxide	CuO/ZnO	200–400	4000 ppm	1.5 min	[63]
	Bi_2O_3 + SnO_2	200–350	< 500 ppm	80–90 s	[64]
	SnO_x	200–500	1–100 ppm	1 min	[65]
	SnO_2	131–313	1–20 ppm	1 h	[66]
	SnO_2	25–400	200–3000 ppm	1 min	[67]
	SnO_2	200–420	50–420 ppm	5 ms	[68]
Ethanol	CuO	350	1–1000 ppm	–	[70]
	Ga_2O_3 +Rh, Ru, Ir	540–800	25–50 ppm	1 min	[71]
	ZnO +SnO_2	20	0.1–5 ppm	–	[72]
	Fe_2O_3 + SnO_2	170–340	10–1000 ppm	–	[73]
	TiO_2	200–400	400–2000 ppm	3 min	[74]
	TiO_2 + Pt/Nb	300–500	500–1250 ppm	5 min	[75]
Hydrogen Sulphide	CeO_2 + SnO_2	10–125	5–25 ppm	30 s	[76]
	CuO + SnO_2	100	5–100 ppm	60–140 s	[77]
	SnO_2	300–350	0–9 ppm	–	[78]
	ZnO + Sb_2O_5	200–400	0.01–40 ppm	15 min	[79]
Humidity (Water vapour)	Ta_2O_5	400–450	45–100% RH	40 ms	[80]
LPG	$ZnGa_2O_4$	200–400	500 ppm	1 min	[81]
Methanol	TiO_2	200–400	100–500 ppm	3 min	[74]
Ammonia	Cr_2O_3 + TiO_2	200–500	10,000 ppm	2–5 min	[82]
	CoO_x	27	1–200 ppm	2–4 min	[83]
	MoO_3	450	3–400 ppm	1 min	[84]
Nitrous oxides	SnO_2	131–313	0.01–0.25 ppm	1 h	[66]
	SnO_2	300–350	0–9 ppm	–	[78]
	SnO_2	200–420	1–2 ppm	5 ms	[68]
	SnO_2	–	100 ppb	–	[85]
	SnO_2	100–350	5–800 ppb	30 min	[86]
	CoO + In_20_3	125	100 ppm	4 min	[87]
Ozone	In_2O_3 + Fe_2O_3	300–550	10–300 ppb	2 min	[88]
Petrol	SnO_2	20–320	1500 ppm	–	[89]
Propane	In_2O_3	350	1000 ppm	1.5 min	[60]
	ZnO	300	0–8000 ppm	–	[90]
Propanol	TiO_2	200–400	400–200 ppm	3 min	[74]
Trimethyl amine	SnO_2	290	10–300 ppm	12 s	[91]
	In_2O_3	300–640	–	–	[69]
Xylene	SnO_2	–	10–100 ppm	10 s	[92]

number of published research on MOx sensors, this list is not exhaustive.

From Table 2, it can be observed that the most commonly sensed gases are carbon monoxide (CO) [63–68] and nitrous oxides (NO, NO_2, NO_x) [66, 68, 78, 85, 86] which are fairly small molecule gases. MOx based sensors for slightly more complex molecules such as Xylene [92], trimethylamine [69, 91] are not that common. While sensitivities down to 5 ppb for some gases have been realized with MOx sensors, the selectivity of this sensing architecture is poor. As observed from the table, the similar fabricated tin oxide (SnO_2) based sensors show a wide range of response to gases such as butane [61], carbon monoxide [64–68], ethanol [72, 73], ammonia, nitrous oxides at similar operating temperatures but with relatively varying response times. Being capable of synthesizing into nanostructured crystalline materials for integration in MEMS devices for improved sensitivity and lower operating temperatures with very low power consumption, as demonstrated by Bhattacharyya et al. [93], these devices show a huge potential for integration into many devices.

3.1.2 Conducting polymers

Conducting polymers are relatively newer functional materials compared to MOx that have been employed as gas sensors since early 80s [94]. As opposed to MOx based gas sensors that operate at high temperatures, CPs have demonstrated better response to target analytes at room temperatures with improved sensitivities and shorter response times. With good mechanical properties and artificial synthesis process to control the electrical properties, CPs have in some cases demonstrated better and more tuneable response than those which can be obtained from traditional MOx based sensors. These conducting polymers are long chain polymers with alternating single (σ) and double (σ–π) bonds. The alternating structure with loosely bonded π electrons that can shift between the bonds as shown in Fig. 3, results in the formation of delocalized π electrons clouds which make them intrinsically conducting.

Through doping and functionalization processes, the behaviour of the conducting polymer can be chemically controlled better than MOx. Synthesis techniques of conducting polymers have been vastly improved from early electrochemical deposition processes, such as those demonstrated by Lu et al. [95], to highly controlled three-dimensional patterning down to microstructure levels as demonstrated by us previously [96, 97], which allow fabrication of more complex sensor architectures using these functional materials. CPs such as polyaniline (PAni), polythiophenes (PTh) and polypyrrole (PPy) are the most widely researched CPs owing to their excellent electromechanical properties. Upon exposure to similarly reducing or oxidizing gases, similar

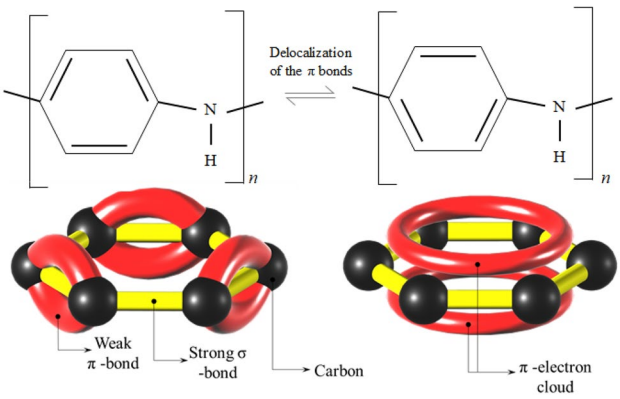

Fig. 3 Above: PAni's structure's alternating double and single bonds showing delocalization induced movement of the π-bond electrons. Below: 3D representation of a π-electron cloud as a result of delocalization

to MOx based sensors, the change in the electrical response of these functional materials have been successfully read out to sense and quantify the volatile concentration. Table 3 summarizes some of the developed CP gas sensors and their characteristic properties for sensing gases.

Although CP gas sensors have quicker response-times sensors with noticeably better sensitivities, the recovery following removal of the gases takes a much longer time compared to MOx sensors, which have similar adsorption and desorption rates. All laboratory results of the recovery following exposure to gases are measured by flushing the sensing element with an inert gas such as argon or helium [98–109]. This is to ensure the complete removal of residual sensed gas not only from the chamber but from the CP sensing element as well. Repeatable exposure to the same gases has also been observed to induce permanent irreversible reaction of the gas to the CP [110].

3.1.3 Carbon nanomaterial and carbon composites

Among carbon based nanomaterials, the most widely researched materials for their gas sensing properties are carbon black (CB), carbon nanofibers (CNF), carbon nanotubes (CNT) both single-walled (SWCNT) and multi-walled (MWCNT) and graphene (Gp). These nanomaterials are typically used in a composite matrix, except for CNTs, which are sometimes used in form of composites, electrospun fibres [111] or as freestanding forests, either in their pristine form or as functionalized/decorated with other nanoparticles [112]. CB and CNF in the form of CB/polymer and CNF/polymer composites have also been demonstrated for gas sensing applications. A schematic representation of the sensing mechanism CB/polymer composites is shown in Fig. 4a. A predetermined amount of CB dispersed into an insulating polymer matrix is laid out as thin films. The CB's mass

Table 3 Conducting polymer based gas sensors and their operating parameters

Gas Sensed	Functional CP	Detection limits	Response time	Recovery time	References
Acetone	PTh	200–300 ppm	3–5 min	3–5 min	[98]
Ammonia	PAni	50 ppb	1–5 min	3 h	[99]
	PPy	38–290 ppm	20 s	15 min	[100]
Carbon monoxide	PAni	10 ppm	5 s	7 s	[101]
	PAni	60 ppm	24 s	36 s	[102]
Carbon dioxide	PPy	100–700 ppm	210–270 s	25–30 min	[103]
Hydrochloric acid	PAni	200 ppb	6 s	10 s	[104]
Hydrogen Sulphide	PAni	10 ppm	1.1 min		[105]
Methanol	PAni	1 ppm	2–20 s	2–15 s	[106]
Nitrous oxides	PPy	20 ppm	< 5 s	4–5 min	[107]
	PTh	4 ppm	< 1 min	10 min	[108]
	PAni	500 ppb	30 s	65 s	[102]
Toluene	PTh	20 ppm	3–5 min	3–5 min	[98]
Water vapour	PAni	25–400 ppm	3–10 s	3–10 s	[109]

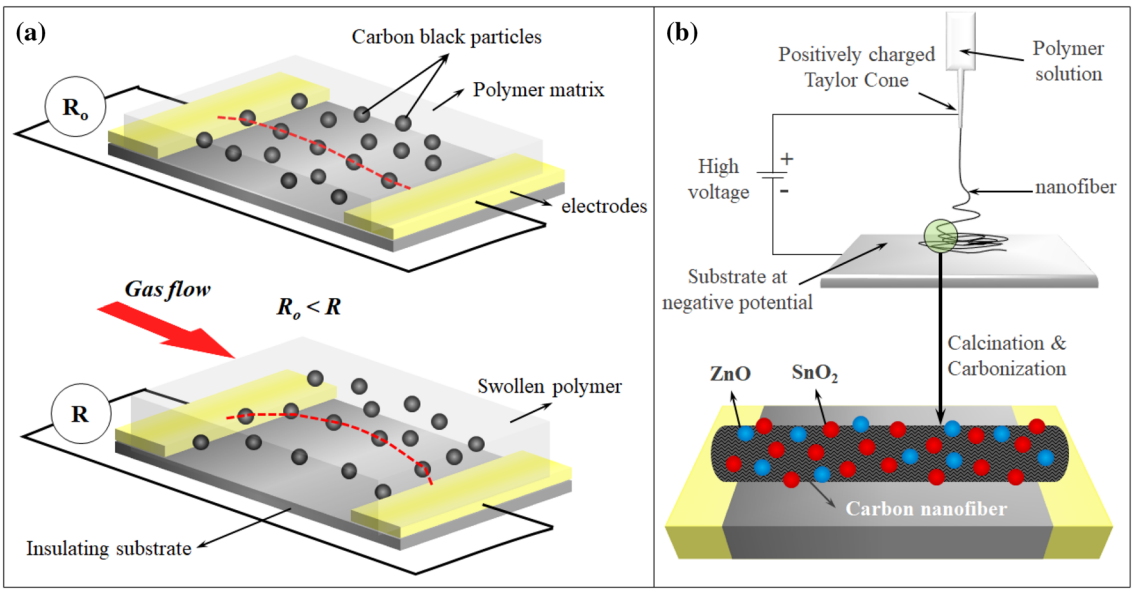

Fig. 4 **a** CB/polymer composite gas sensor swelling under gas flow increasing sensor resistance. **b** MOx coated electrospun CNT for gas sensing

fraction would characterize the electrical properties of the film, which is defined by percolation theory [113]. The target volatile determines the chemical composition of the insulating polymer matrix as the polymer matrix needs to swell in presence of the target volatiles. Once the CB/polymer composite sensor is synthesized, in presence of the target volatile the polymer matrix swells. This increases the anti-particle distances between the conductive CB particles thus increasing their tunnelling resistance as shown in Fig. 4a.

Using an array of swelling polymers composed of vinylated phenols, styrene–co-alcohols, acrylates and bis-phenols, Lonergan et al. [114] demonstrated that the CB/polymer composites were capable of responding to a wide range of volatile organic compounds among which the characteristic response of individual CB/polymers to toluene, methanol, 2-propanol, hexane, ethyl acetate, ethanol, chloroform, benzene and acetone were analysed. As the insulating polymers in the composites swell differently to different volatiles, the consolidated responses were identified through principal component analysis [114]. Once the CB/polymer sensing array elements were characterized, to identify the type of volatile present, a simple cross reference to the previously established principal component space is carried out. However, the macromolecular movement of the CB within the matrix results in rearrangement of this conductive filler within the polymer matrix thus

inducing a steady signal drift upon consecutive swelling and shrinking process.

With relatively low sensitivity of CB/polymer composites (in few parts per thousand ranges), research into CNF/polymers based sensors synthesized in a similar fashion were carried out [115, 116]. While pristine CNF/polymer gas sensors show stable performance due to increased resistance to macroscopic movement of the high-aspect ratio fibres [115], works by Zhang et al. [117] and Lee et al. [118] demonstrate use of metal and metal oxide decorated CNFs fabricated through electrospinning technique to further improve the sensitivity of their gas sensors. A schematic representation of this sensing architecture is shown in Fig. 4b. ZnO and SnO_2 decorated electrospun CNFs were directly deposited as thin films without the need for an insulating matrix. This allowed direct contact of the target volatiles to these functional materials. Dimethyl methyl phosphonate were detected down to 0.1 ppb using this sensor [118].

Numerous SWCNT and MWCNT based gas sensors have also been developed alongside CB and CNF based sensors. Earliest research using SWCNTs as gas sensors, that are capable of responding to nitrous oxide and ammonia vapours, was carried out by Tan et al. [119]. By fabricating a transistor like architecture using the vapour sensitive SWCNT as the transistor base layer, Kong et al. [120] demonstrated increase in conductance by nearly a factor of 10 upon exposure to 200 ppm NO_2 gas. Upon exposure to 1% NH3 in Argon, the conductance of sensor nearly dropped to zero. The turn on time upon exposure to NO_2 was less than 5 s while the turn off time upon exposure to NH_3 was about 3 min. While Palladium (Pd) functionalized CNT gas sensors showed high sensitivities to hydrogen [121], CNT's decorated with metals such as but not limited to Zn, Cr, Pt, Rh demonstrated improved sensitivities to CO, NO2 methane and hydrogen sulphide and benzene. Rh-CNT gas sensors were fabricated by Leghrib et al. [122] for detecting benzene vapours. The Rh-CNT gas sensors were exposed to benzene as low as 50 ppb with a sensor response time of less than a minute. To remove the benzene from the Rh-CNT, the setup was heated to 150 °C and this resulted in a nearly instantaneous drop in resistance. For successive exposure to benzene vapours, the Rh-CNT sensor was required to be brought to room temperature, which took over 10 min [122].

Gp based gas sensors are relatively new with the first reported use being as late as 2007 compared to other carbon nanoparticles [123]. Similar to performance levels of CNT gas sensors, Gp gas sensors also required reheating following sensing of target gases. With doping and nanoparticle decoration to enhance carbon nanoparticle properties having already been demonstrated in the field of CNF and CNT based sensing applications, boron or sulphur doped Gp were identified in silico to be capable of detecting nitric oxides [124]. With further research into reduced graphene oxide (rGpO), Pd nanoparticle decorated rGpO sensors were fabricated by Li et al. [125] using chemical vapour deposited Gp sheets as the contact material for the Pd-rGpO sheets. The demonstrated sensor showed high levels of sensitivity (2–420 ppb) to NO gas with 50 min response and 45 min of recovery time.

3.2 Metal organic frameworks and covalent organic frameworks

Metal organic frameworks (MOFs) and covalent organic frameworks (COFs) are a new class of functional materials that have diverse assembly of building units similar to zeolites [126]. Research into MOFs has exploded since their inception owing to their high-density storage capabilities of gases like H_2 and CH_4. MOFs are in essence a highly structured (2D and 3D) and nanoporous network of polyatomic metallic clusters linked together by polytopic linkers [127–129]. Numerous reviews published on this class of functional material [130, 131] exploring their possible applications as gas storage media in transportation and chemical processing plants and a large database on various MOFs indicate their extremely selective and robust gas storage capabilities.

The controlled nanoporous structure makes MOFs extremely selective to a particular chemical, a feature that has been exploited for use as chemical sensors. When chromophores (a colour producing atom/group) are used as linkers for the metallic clusters during the synthesis of MOF, upon exposure to a sorptive fluid, a solvatochormic (in case of liquids)/vapochromic (in case of gases) shift occurs which can be used as an indicator for the presence of the sorptive fluid. Lu et al. have synthesized a Cu-MOF containing 3, 6-di (pyridine-4-yl)-1, 2, 4, 5-tetrazine as the polytopic linker which can produce a solvatochormic shift in the visible spectrum when exposed to different organic compounds [132]. Upon exposure to acetonitrile, the synthesized MOF appears as bright red while exposure to trichloromethane results in absorption of all wavelengths of the visible spectrum except dark green. Among various sensing approaches using MOF under the presence of a sorptive fluid as reviewed by Kreno et al., [133], the most idealistic form of implementation of these MOF sensors in sensing pathogenic biomarkers can be through use of micro-cantilever structures (MCLs) as demonstrated by Lee et al. [134]. These MCLs comprises an extremely thin coating of a suitable MOF (MOF selection depends on the target volatile to be sensed) on a MCL with highly sensitive piezoresistive elements patterned using photolithography techniques. During sorption of target gases, the changes in unit cell dimensions result in a large tensile and compressive stress on the cantilever and this change in stress is measured by the piezoresistive element as schematically represented in Fig. 5.

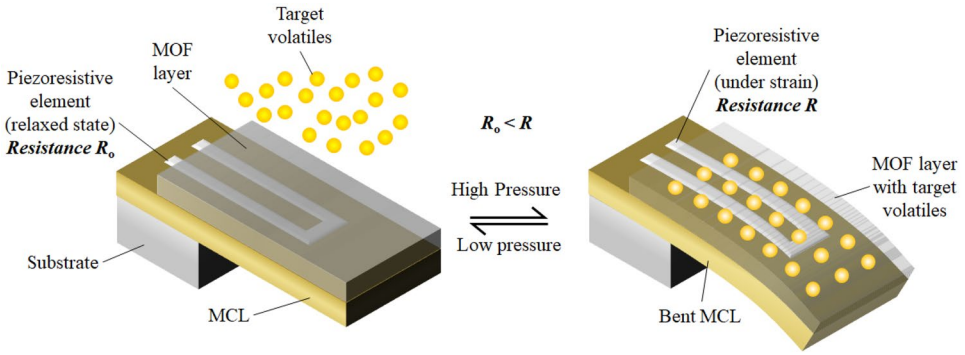

Fig. 5 Piezoresistive MCL with MOF coating showing adsorption induced response change for gas sensing

Similar to MOFs, COFs are made up of porous crystalline polymers that are linked together via covalent bonds. The ability to synthesize these COFs akin to MOFs with relatively higher mechanical and thermal stability due to strong covalent bonds makes this material more attractive than MOFs [135]. With all the advantages of MOFs, COFs have also been increasingly synthesized since first reported in 2005. A detailed review of various COFs with their chemical structures and properties has been carried out by Ding and Wang [136] and Feng et al. [137].

It is only as recent as the early 2010s that the potential of these COFs as a sensing element has been reported. The first potential use of COFs as a sensing element for 2, 4, 6-trinitrophenol (TNP) was proposed and identified by Das et al. [138]. Using TfpBDH covalent organic nanosheets, the group was able to visualize a complete shift in the spectral emission of the pristine nanosheet turning it from a bright blue sheet to a dark bluish grey sheet upon exposure to TNP [138]. This process was identified to be reversible upon exposure to triethylamine. The colour shift occuring within 36 ns when exposed to TNP indicated extremely fast response times. With the group focusing primarily on COF synthesis, only a part of their research was on using the synthesized COF as a TNP sensor.

A more detailed research on using COFs as a sensor was carried out by Li et al. [139] for detecting copper ions (Cu^{2+}). Solvothermally synthesized COF-JLU3 was used as the sensing COF with fluorescence shift based visual detection upon exposure to Cu^{2+} ions. The luminescence spectra of COF-JLU3 suspension in tetrahydrofuran changes shows the peak intensity at 601 nm drop from 100 a.u (normalized intensity) down to 10 a.u in the presence of Cu^{2+} ions. The selectivity of COF-LJU3 to Cu^{2+} ions were verified by testing and measuring their intensity shift with other metallic ions such as lead, silver, potassium, sodium ions. While most of the tested ions showed only less than 20% drop in the normalized luminous intensity, the COF-JLU3 also demonstrated up to 60% drop in presence of nickel, iron and cobalt ions.

Ding et al. [140] used COF-LZU8 to develop fluorescent COFs specifically for sensing and removal of mercury ions (Hg^{2+}). The COF-LZU8 was functionalized with thioether group for improving the selective detection and facile removal of Hg^{2+}. The thio ether group was used as the Hg^{2+} receptor and the porous structure of the framework for real-time detection. With high levels of reported sensitivity (spectral shift occurs at concentrations as small as 3.3 µM with 90% drop at 33.3 µM) and excellent selectivity (less than 15% spectral intensity drop to all other metallic ions tested [140]) the fluorescent COFs enabled easy visibility of the COFs real-time response. This research highlights the construction of functionalized COFs that can further open up these functional materials to a wider range of applications.

3.3 Hydrogels and hydrogel composites

Hydrogels are highly hydrophilic polymeric structures that upon exposure to water can swell by absorbing the water until an equilibrium state is attained. Hydrogels are themselves not a singular polymeric compound but a generalized term that encompasses all hydrophilic swell-able polymeric networks [141]. Their chemical characteristics have made them an ideal candidate for use as sensing materials and we focus on research that has been carried out using these materials as chemical sensors.

Using a MCL type architecture, pH sensitive poly (vinyl alcohol)/poly (acrylic acid) (PVA/PAA) hydrogels have been used to sense chemicals with pH levels of 7 (neutral) and 1 (strong acid) [142]. A 50 µm thick PVA/PAA hydrogel layer was deposited on a MCL with a piezoresistive bridge network fabricated using photolithography. Upon exposure to a fluid with a low pH, the hydrogel shrinks rapidly inducing a shift of the mass of the hydrogel film on the MCL. This resulting drop in output voltage is picked up by the electronics as a presence of strong acid. The extent of shrinkage depends on the strength of the acid that has been calibrated against the output voltage of the sensor demonstrating a hydrogel based pH sensor with a sensitivity of 15 mV/pH.

Trinh et al. [143] further analysed the behaviour of these hydrogels under varying pH conditions in silico. Similar research with bilayer cantilevers with hydrogels coated on either side was also demonstrated to detect pH changes [142].

Gas sensing with hydrogels has also been demonstrated by modifying the hydrogel with gas sensitive fluorescent dyes [144, 145]. Using 4-amino, 5-methylamino, 2′, 7′-difluorofluorescein within a polyethylene glycol hydrogel, Zguris J et al. [145] were able to demonstrate fluorescence shift upon exposure to NO. The use of fluorescent dye did not affect the molecular structure of the hydrogel. It allowed the shift of colour within the hydrogel even at exposure limits as small as 0.5 µM. Exploiting this bio-inert character of hydrogels, the use of sodium bicarbonate in a pH-sensitive hydrogel sensor allowed sensing of CO_2 gas directly without dissolution in fluids as demonstrated by Herber et al. [146].

Efforts to bring together multiple sensing elements have been demonstrated by Bai et al. [147] where graphene oxides (GpO)/CP composites based hydrogels were developed. These hybrid hydrogels were prepared by in situ chemical polymerization in aqueous dispersions of GpO sheets. Three different conducting polymers namely PAni, PPy and poly (3, 4-ethylenedioxythiophene) (PEDOT) grafted with GpO based hydrogels were synthesized with GpO/PPy based hydrogels demonstrating high sensitivity to ammonia gas at concentrations down to 800 ppm. The sensor was fabricated by using the hydrogel film in-between two conductive electrodes as a chemoresistor and demonstrated response times less than 10s. While the recovery rate after removal of ammonia is not detailed, the high electrical conductivity due the presence of GpO and CPs within the hydrogel, and the bio-inert nature of hydrogel demonstrates huge potential for use of these hybrid composite hydrogels as an electroactive material in biomedical applications.

More recently, Wu et al. [148] have developed a high performance CO_2 and NO_2 sensor with three-dimensional functionalized rGpO based hydrogels using molecular self-assembly in presence of hydroquinone. The group compared functionalized and non-functionalized rGpO based hydrogels and determined that functionalized rGpO exhibits comparatively faster recovery times (10 min) and lower detection limits (NO_2 at 200 ppb and CO_2 at 20 ppm). The works by Bai et al. [147] and Wu et al. [148], demonstrate that hybrid sensor designs using multiple functional materials can alleviate the drawbacks of either functional material allowing better sensing architectures to be realized.

3.4 Synthetic oligomers

Single stranded deoxyribose/ribonucleic acids (ssDNA/ssRNA), or more commonly, aptamers, are specifically isolated strands from a large chemically synthesized oligonucleotide library on the basis of their affinity to a specific target molecule [149, 150]. When an aptamer is required for a specific target molecule, a process called systemic evolution of ligands by exponential enrichment or SELEX is used, where the target molecule in a suitable solvent is introduced into a large library (in the order of 12–15) of oligonucleotides. The single strands, which have the highest affinity to the target molecule, bind to the introduced target molecule. The unbound ssDNA are washed away and the bound ssDNA are enriched through polymerase chain reaction (PCR) amplification and purification as shown in Fig. 6a. The process is repeated until only ssDNA with the highest affinity to the target molecule remains. As the SELEX process can be tailored to suit a wide range of molecules and with techniques such as flu-mag-SELEX [151] and other non-SELEX based aptamer selection techniques [152], the target molecule range has been widely extended. These biomaterials are capable of completely folding around their target molecule at suitable pH conditions and can reverse the folding process to release the target molecule at certain pH as shown in Fig. 6b or by reversing the electric potential.

The synthesis of these aptamers tailored to a specific target molecule introduces extremely high selectivity and their

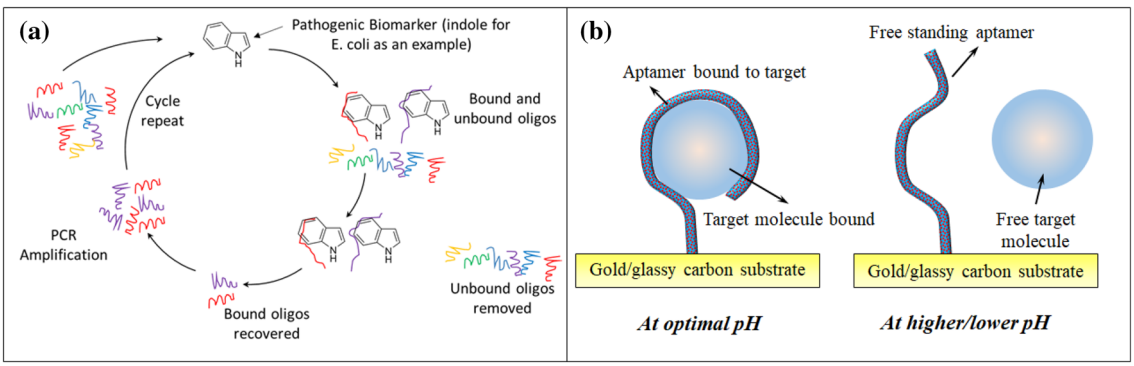

Fig. 6 **a** Aptamer selection through SELEX process **b** reversible action of aptamer binding to target molecule through pH control

intrinsically high sensitivities (with molecular level folding) make these synthetic materials as a highly potent chemical sensor. Their high levels of biocompatibility have already been utilized in synthesis of automated drug delivery devices in vivo [153–155]. For instance, Huang et al. [155], have demonstrated conjugation of anti-tumour drugs to target the antibodies by attaching the drugs to an aptamer designed for targeting tumour cells. Sgc8 aptamer [156], was truncated to form Sgc8c [155] to specifically target the protein, tyrosine kinase 7. This protein is specifically expressed in lymphoblastoids having the T cell acute lymphoblastic leukaemia. Fluorescein conjugated antitumor drug, doxorubicin (DOX), was conjugated to the Sgc8c aptamer and exposed to the T-cells in assays and the activity of the aptamer was monitored. It was observed that the aptamer prevents release of DOX at non-specific sites but unconjugated the drug only upon binding to the target T-cell, thus releasing the drug at T-cell specific sites. Apart from targeted drug delivery applications, aptamers are also starting to see increasing use as an electrochemical sensor for sensing complex proteins to small molecules and ions. Wang et al. [157] have demonstrated the use of aptamers for detecting the enzyme, thrombin at concentrations as low as 0.1 nM. Folate receptors were detected at 0.77 ng/mL by He et al. [158]. Metallic ions such as potassium ions, silver ions and mercury ions have been detected using aptamers down to 100 µM, 5 nM and 0.5 nM respectively [159–161].

While aptamers have exhibited excellent stability and selectivity in liquid phase medium, use of ssDNA to detect gas phase medium was demonstrated by Staii and Johnson [162]. ssDNAs can effectively bind to the target molecule in the same medium selected from the oligonucleotide library. However, by decorating these ssDNA on SWCNT, the researchers managed to demonstrate acceptable levels of response from ssDNA decorated SWCNT to various gases (the schematic of the senor setup is shown in Fig. 7). By passing propionic acid vapours at 150 ppm, over bare and ssDNA decorated SWCNT based sensors the researchers observed over 8% variation in the current transfer ratio [162]. A stronger response was however observed upon the sensor being exposed to trimethylamine when a difference of 30% in current transfer ratio was observed between the bare and ssDNA decorated SWCNT indicated a better selectivity towards trimethylamine. While the reported response indicates a severe drop in selectivity and sensitivity of ssDNAs while operating in air, the research promises potential for future improvement in in-air volatile sensing capabilities of ssDNAs.

As a means of infection sensing, aptamers have also been demonstrated to be capable of sensing *E. coli* and *S. aureus*. The aptamers are selected from the oligonucleotide libraries by using *E. coli* and *S. aureus* as the binding targets. So et al. [163] have demonstrated the use of aptamer functionalized SWCNTs (apt-SWCNT) to screen for presence of *E. coli* for eventual application in testing food samples. Using arrays of apt-SWCNT as field effect transistors that show a conductance decrease of more than 50% upon binding with *E. coli*, So et al. have been able to demonstrate rapid detection (< 20 min) of *E. coli*. By using *Salmonella* as a control to observe the apt-SWCNT sensor's response in non *E. coli* solutions, the selectivity of the sensor was demonstrated. A dense array of apt-SWNCT to maximize the surface area was also proposed towards development of a more rapid screening tool.

S. aureus Aptamer/Gp based piezoelectric sensor was developed by Lian et al. [164] for rapid and specific detection of *S. aureus*. The aptamer/Gp was electrochemically deposited onto interdigital gold electrodes that were connected to a piezoelectric quartz crystal. Upon binding of the aptamers with *S. aureus*, the shift in electrical parameters resulted in change of resonance frequency of the quartz crystal that was used as a response for *S. aureus* presence. With a short response time of 60 min, the sensors demonstrated high levels of sensitivity (detection limits as small as 41 CFU/mL). These aptamer sensors [163, 164] though capable of detecting *E. coli* and *S. aureus* with high levels of selectivity and sensitivity demand the pathogens to be in a suitable buffer.

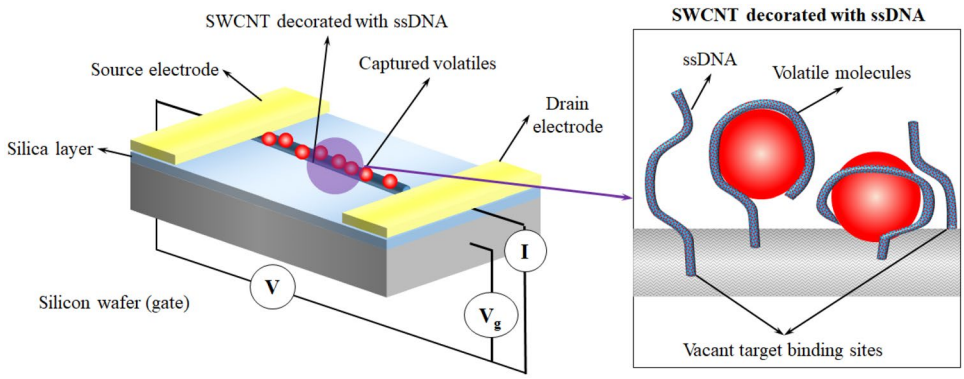

Fig. 7 Device architecture of ssDNA decorated SWCNT gas sensors

3.5 Insect odorant receptors

With attractive properties of using biomaterials such as aptamers for sensing, a more recent and novel approach involves utilizing biomaterial from living beings, in particular insects, as electrochemical sensor to explore the possibility of biomimicking the process of 'smell'. Insects among many organisms possess a heightened sense of smell [165]. The olfactory sensory neurons of the insect antennae have membrane proteins acting as odorant receptors [166]. Montage et al., have analysed these odorant receptors expressed in cell lines and observed their sensitivity to various compounds [167]. These odorant receptors are a family of G protein-couple receptors, which unlike aptamers that are capable of binding to ligands and small molecules, display extreme affinity to a range of odour molecules. Recent research on odorant receptor grafted liposomes bound covalently to gold electrodes has demonstrated to be capable of detecting 4-ethlyguaiacol (4-EG), an odorant molecule released from wine and beer [168]. Using odorant receptors from the common fruit fly, *Drosophila melanogaster*, detection limits as low as 1aM were realized (10^{-18} mol/l) [168]. While the odorant receptors showed positive response to 4-EG no response was observed when exposed to E2-hexenal which is also an odour compound with a leaf-like odour.

4 Conclusion and outlook

The unique electrochemical properties and the electronic structure of novel functional materials are being constantly improved upon and newer gas sensing capabilities are being explored. Existing literature indicates that the implementation of these novel functional materials for sensing infections has not been thoroughly explored with an increasing need for further intrinsic improvements to eliminate their various drawbacks. The unique nature of the reviewed functional materials allows their synthesis into flexible/elastic matrices to act as a secondary skin that wraps around the wound-prosthesis interface. Some sensing architectures, such as carbon nano-particle/swelling polymer based sensors and piezoresistive cantilever MOFs sensors, though operate on the principle of the functional material expanding and contracting can still be used as a flexible secondary skin through prior electronic calibration. Furthermore, the sensing techniques and sensor architectures reviewed here allow realization of an integrated sensor with low power requirements (in the order of few microwatts to few milliwatts) to enable these sensors to draw power from portable energy sources (batteries or motion powered energy harvesters) that can be integrated into osseointegrated prosthesis. A brief summary of various sensing architectures reviewed and their salient features are detailed in Table 4.

Implementing MOx in infection sensing applications would demand sensing a very narrow range of pathogenic volatiles, more particularly in close proximity to soft tissues. However, this is hindered by their poor selectivity and high operating temperatures. As pathogenic volatiles are an extremely complex mixture of various commonly occurring gases such as CO_2, NO_X, amongst other pathogen specific biomarkers [49–52], the MOx sensors would be exposed to more than one type of oxidizing/reducing gases at the same time and the electron transfer strength of these gases can greatly influence the gas to which MOx sensor responds to. In such cases where competing gases are to be selectively detected, a largely varied array with each sensing element having unique operating temperatures for tuned selectivity becomes necessary to be able to sense a specific pathogenic biomarker making this functional material an unrealistic choice for precision sensing of infection with zero false positives.

As for CPs, the requirement of flushing the sensing element with an inert gas after interaction with the target gas, to ensure a faster and near complete recovery, requires

Table 4 Comparative overview of sensing architectures for potential use as pathogenic biomarker sensors

Functional material	Selectivity	Sensitivity	Response times	Operating voltages	Biocompatibility	Degradability
MOx	Poor	5 ppb–10 ppt	5 ms–30 min	− 20 to 20 V	Low	Low
CP	Poor	50 ppb–700 ppm	< 5 s (response) 30 min (recovery)	10 V	High	Medium
Carbon nanoparticle composites	Poor	0.1 ppb–420 ppb	50 min	Resistive (5 V bias	Low (CNT-carcinogenic)	Medium
MOFs	Good	5 ppb–40 ppm	20 s–5 min	Resistive (5 V bias)	Good	Medium
COFs	Good	2.8 pg/mL	40 ns	0.6 V	Good	Medium
Hydrogel/hydrogel composites	High	1–10 ppm	Continual rise > 10 min	~ 125 mV	High	High
Synthetic oligomers	Extremely High	1 fM	Exposure 30–60 min	N/A (EIS at 1.02 V)	High	High
Insect odorant receptors	High	1 aM (attomolar)	Exposure 15 min	N/A (EIS at 1.02 V)	High	High

additional inert gas storage media to be introduced into portable sensors for use in remote infection sensing applications. The long-term instability and irreversibility coupled with selectivity issues akin to MOx based sensors further renders this functional material unsuitable for applications demanding a high level of selective volatile sensing but the fast response time makes certain aspects of this functional material worth further research.

Carbon nanoparticle based gas sensors demonstrate comparable sensitivities and response times to that of CP based sensors and at the same time provide long-term stability. However, the comparatively slower relaxation times coupled with carcinogenic nature of freestanding nanoparticles [169] makes these functional materials less attractive for use in biomedical applications such as infection sensing where they would be in close proximity to humans. However, research into the biocompatible elastomer encapsulated sensors fabricated from these carbon nanoparticles demonstrate a good fit for biomedical applications [20] making them an ideal choice for conductive electrodes that can conform to the prosthetic's movements. These three most commonly used functional materials in E-nose applications demand having an array architecture as they suffer from low selectivity. Furthermore, only research on simpler volatile compounds has been demonstrated, demanding further improvement in this field for detecting complex organic volatiles.

MOFs and COFs show high sensitivities and selectivity to the target molecules with ease of chemical synthesis in laboratory environment and their high levels of tenability make them an ideal candidate for potential use in infectious biomarker sensing applications. With higher thermal stability than MOFs, the more recently introduced COFs are especially a highly promising source for future research and application as a gas sensing media. Although sensors have been demonstrated using the COFs for sensing ions liquid phase, the atmospheric pressure conditions lower the amount of target molecules adsorbed into the framework demanding the need for higher atmospheric pressures.

While hydrogels on their own have limited potential for gas sensing and lower stability in atmospheric conditions with evaporation induced sensor degradation, pioneering works by [147] and [148] demonstrate the capabilities of combining multiple functional materials to enhance their characteristics.

The high selectivity and sensitivity of aptamer show a huge promise for detecting specific volatiles such as pathogenic biomarkers. The advancements in SELEX processes to identify aptamers for a specific molecule would allow rapid synthesis of aptamers specific to individual pathogenic biomarkers. By using an array of individual pathogenic biomarker binding aptamers, an infection sensor capable of sensing pathogens at early stages of infection would be possible, in addition to aiding in diagnosis of the pathogen itself. The limitations of realization of such sensors, at present, are primarily due to inability to maintain aptamer sensors in their synthesis buffer (liquid) media while being exposed to the target pathogenic biomarkers as a solid-state sensing media.

With the introduction of aptamer based biomaterial sensors and the more recent use of olfactory receptors from insects, the potential for new and more effective sensors capable of detecting infections is on the rise. The ideal pathogenic biomarker sensors should have the selectivity of aptamers, with sensitivity of odorant receptors and a long-term stable configuration in a solid-state architecture like those of MOx, CP and carbon nanoparticle based sensors. Furthermore, the organic nature of these DNA based functional materials (aptamers and olfactory receptors) introduces innate biocompatibility when these materials are integrated into flexible wearable sleeves that can encapsulate the wound-prosthesis interface. While olfactory receptors are extremely sensitive to target molecule, unlike aptamers, they are not custom synthesizable to target a specific molecule making the selectivity and tuneability of aptamers worth future research for infection sensing applications. It can be anticipated that further research into these functional materials for potential use in infection sensing applications can reveal highly capable sensing architectures and pave a pathway for future volatile sensors.

Having identified the salient features of various functional materials and their drawbacks, the aim of this review is to promote research and development of more novel sensing mechanisms. Combining the promising features of the current state-of-art functional materials would allow realization of a superior class of functional materials for use in infection sensing in biomedical devices and across a wider range of applications.

Acknowledgements The review of existing literature for this article was carried out with funding from US Office of Naval Research (Grant Number N62909-17-1-2014).

Compliance with ethical standards

Conflict of interest The authors declare no conflicts of interest.

Ethics approval The article does not contain any studies with human or animal participants that were carried out by the author.

References

1. Seymour R. Prosthetics and orthotics: lower limb and spinal. Philadelphia: Lippincott Williams & Wilkins; 2002.
2. Magee R. Amputation through the ages: the oldest major surgical operation. Aust N Z J Surg. 1998;68(9):675–8.

3. Fite K, Mitchell J, Sup F, Goldfarb M, editors. Design and control of an electrically powered knee prosthesis. In: 2007 IEEE 10th international conference on rehabilitation robotics. IEEE; 2007.
4. Mavroidis C, Pfeiffer C, DeLaurentis KJ, Mosley MJ. Prosthetic, orthotic, and other rehabilitative robotic assistive devices actuated by smart materials. Google Patents; 2002.
5. Carlson JD, Matthis W, Toscano JR, editors. Smart prosthetics based on magnetorheological fluids. Smart structures and materials 2001: industrial and commercial applications of smart structures technologies. International Society for Optics and Photonics; 2001.
6. Leong J, Parzer P, Perteneder F, Babic T, Rendl C, Vogl A, et al., editors. proCover: sensory augmentation of prosthetic limbs using smart textile covers. In: Proceedings of the 29th annual symposium on user interface software and technology. ACM;2016.
7. Finch J. The ancient origins of prosthetic medicine. Lancet. 2011;377(9765):548–9.
8. Thurston AJ. Paré and prosthetics: the early history of artificial limbs. ANZ J Surg. 2007;77(12):1114–9.
9. Herbert N, Simpson D, Spence WD, Ion W. A preliminary investigation into the development of 3-D printing of prosthetic sockets. J Rehabil Res Dev. 2005;42(2):141.
10. Simone F, York A, Seelecke S, editors. Design and fabrication of a three-finger prosthetic hand using SMA muscle wires. In: Bioinspiration, biomimetics, and bioreplication. International Society for Optics and Photonics; 2015.
11. Bahari MS, Jaffar A, Low CY, Jaafar R, Roese K, Yussof H. Design and development of a multifingered prosthetic hand. Int J Soc Robot. 2012;4(1):59–66.
12. Campbell T, Williams C, Ivanova O, Garrett B. Could 3D printing change the world. Technologies, Potential, and Implications of Additive Manufacturing, Atlantic Council, Washington, DC. 2011:3.
13. Dodziuk H. Applications of 3D printing in healthcare. Pol J Cardio-thoracic Surg. 2016;13(3):283.
14. Childress D, Steege J. Computer-aided analysis of below-knee socket pressure. J Rehabil Res Dev. 1987;25(1):22–4.
15. Silver-Thorn B, Childress DS. Parametric analysis using the finite element method to investigate prosthetic interface stresses for persons with trans-tibial amputation. J Rehabil Res Dev. 1996;33(3):227–38.
16. Sonck WA, Cockrell JL, Koepke GH. Effect of liner materials on interface pressures in below-knee prostheses. Arch Phys Med Rehabil. 1970;51(11):666.
17. Appoldt FA, Bennett L. A preliminary report on dynamic socket pressures. Bull Prosthet Res. 1967;10(8):20–55.
18. Convery P, Buis A. Socket/stump interface dynamic pressure distributions recorded during the prosthetic stance phase of gait of a trans-tibial amputee wearing a hydrocast socket. Prosthet Orthot Int. 1999;23(2):107–12.
19. Biddiss E, Chau T. Electroactive polymeric sensors in hand prostheses: bending response of an ionic polymer metal composite. Med Eng Phys. 2006;28(6):568–78.
20. Devaraj H, Giffney T, Petit A, Assadian M, Aw K. The development of highly flexible stretch sensors for a robotic hand. Robotics. 2018;7(3):54.
21. Young AJ, Simon AM, Fey NP, Hargrove LJ. Intent recognition in a powered lower limb prosthesis using time history information. Ann Biomed Eng. 2014;42(3):631–41.
22. Leong J, Parzer P, Perteneder F, Babic T, Rendl C, Vogl A, et al., editors. proCover: sensory augmentation of prosthetic limbs using smart textile covers. In: Proceedings of the 29th annual symposium on user interface software and technology. ACM;2016.
23. McColl I. Review of artificial limb and appliance centre services: the report of an independent working party under the chairmanship of Professor Ian McColl. DHSS; 1986.
24. Nielsen CC. A survey of amputees: functional level and life satisfaction, information needs, and the prosthetist's role. J Prosthet Orthot. 1991;3(3):125–9.
25. Lyon CC, Kulkarni J, Zimersonc E, Van Ross E, Beck MH. Skin disorders in amputees. J Am Acad Dermatol. 2000;42(3):501–7.
26. Levy SW. Skin problems of the leg amputee. Prosthet Orthot Int. 1980;4(1):37–44.
27. Meulenbelt HE, Dijkstra PU, Jonkman MF, Geertzen JH. Skin problems in lower limb amputees: a systematic review. Disabil Rehabil. 2006;28(10):603–8.
28. Branemark R, Branemark P, Rydevik B, Myers RR. Osseointegration in skeletal reconstruction and rehabilitation: a review. J Rehabil Res Dev. 2001;38(2):175–82.
29. Adell R, Eriksson B, Lekholm U, Brånemark P-I, Jemt T. A long-term follow-up study of osseointegrated implants in the treatment of totally edentulous jaws. Int J Oral Maxillofacial Implants. 1990; 5(4).
30. Aschoff H-H, Clausen A, Tsoumpris K, Hoffmeister T. Implantation der Endo-Exo-Femurprothese zur verbesserung der mobilität amputierter patienten. Operative Orthopädie und Traumatologie. 2011;23(5):462–72.
31. Aschoff HH, Kennon RE, Keggi JM, Rubin LE. Transcutaneous, distal femoral, intramedullary attachment for above-the-knee prostheses: an endo-exo device. JBJS. 2010;92(2):180–6.
32. Van de Meent H, Hopman MT, Frölke JP. Walking ability and quality of life in subjects with transfemoral amputation: a comparison of osseointegration with socket prostheses. Arch Phys Med Rehabil. 2013;94(11):2174–8.
33. Haggstrom EE, Hansson E, Hagberg K. Comparison of prosthetic costs and service between osseointegrated and conventional suspended transfemoral prostheses. Prosthet Orthot Int. 2013;37(2):152–60.
34. Brånemark R, Berlin Ö, Hagberg K, Bergh P, Gunterberg B, Rydevik B. A novel osseointegrated percutaneous prosthetic system for the treatment of patients with transfemoral amputation: a prospective study of 51 patients. Bone Joint J. 2014;96(1):106–13.
35. Brånemark RP, Hagberg K, Kulbacka-Ortiz K, Berlin Ö, Rydevik B. Osseointegrated percutaneous prosthetic system for the treatment of patients with transfemoral amputation: a prospective five-year follow-up of patient-reported outcomes and complications. J Am Acad Orthop Surg. 2019;27(16):e743–e751. https://doi.org/10.5435/JAAOS-D-17-00621.
36. Aschoff H, Juhnke D. Evaluation of 10 years experience with endo-exo femur prostheses-background, data and results. Zeitschrift fur Orthopadie und Unfallchirurgie. 2012;150(6):607–14.
37. Boyce JM. It is time for action: improving hand hygiene in hospitals. Ann Intern Med. 1999;130(2):153–5.
38. Kramer A, Schwebke I, Kampf G. How long do nosocomial pathogens persist on inanimate surfaces? A systematic review. BMC Infect Dis. 2006;6(1):130.
39. Holmes AH, Moore LS, Sundsfjord A, Steinbakk M, Regmi S, Karkey A, et al. Understanding the mechanisms and drivers of antimicrobial resistance. Lancet. 2016;387(10014):176–87.
40. Gbejuade HO, Lovering AM, Webb JC. The role of microbial biofilms in prosthetic joint infections: a review. Acta Orthop. 2015;86(2):147–58.
41. An YH, Friedman RJ. Concise review of mechanisms of bacterial adhesion to biomaterial surfaces. J Biomed Mater Res. 1998;43(3):338–48.
42. Ohko Y, Utsumi Y, Niwa C, Tatsuma T, Kobayakawa K, Satoh Y, et al. Self-sterilizing and self-cleaning of silicone catheters

coated with TiO_2 photocatalyst thin films: a preclinical work. J Biomed Mater Res. 2001;58(1):97–101.
43. Shirtliff ME, Calhoun JH, Mader JT. Experimental osteomyelitis treatment with antibiotic-impregnated hydroxyapatite. Clin Orthop Relat Res. 2002;401:239–47.
44. Arciola CR, Bustanji Y, Conti M, Campoccia D, Baldassarri L, Samori B, et al. Staphylococcus epidermidis–fibronectin binding and its inhibition by heparin. Biomaterials. 2003;24(18):3013–9.
45. Voller A, Bidwell D, Bartlett A. Enzyme immunoassays in diagnostic medicine: theory and practice. Bull World Health Organ. 1976;53(1):55.
46. Gomez E, Cazanave C, Cunningham SA, Greenwood-Quaintance KE, Steckelberg JM, Uhl JR, et al. Prosthetic joint infection diagnosis using broad-range PCR of biofilms dislodged from knee and hip arthroplasty surfaces using sonication. J Clin Microbiol. 2012;50(11):3501–8.
47. Lee HH, Burczak J, Muldoon S, Leckie G, Chernesky M, Schachter J, et al. Diagnosis of Chlamydia trachomatis genitourinary infection in women by ligase chain reaction assay of urine. Lancet. 1995;345(8944):213–6.
48. Majno G. The ancient riddle of σῆψις (sepsis). J Infect Dis. 1991;163(5):937–45.
49. Bean HD, Dimandja JMD, Hill JE. Bacterial volatile discovery using solid phase microextraction and comprehensive two-dimensional gas chromatography-time-of-flight mass spectrometry. J Chromatogr B. 2012;901:41–6.
50. Cao W, Duan Y. Breath analysis: potential for clinical diagnosis and exposure assessment. Clin Chem. 2006;52(5):800–11.
51. Zhu J, Jiménez-Díaz J, Bean HD, Daphtary NA, Aliyeva MI, Lundblad LK, et al. Robust detection of *P. aeruginosa* and *S. aureus* acute lung infections by secondary electrospray ionization-mass spectrometry (SESI-MS) breathprinting: from initial infection to clearance. J Breath Res. 2013;7(3):037106.
52. Devaraj H, Pook C, Swift S, Aw KC, McDaid AJ. Profiling of headspace volatiles from *Escherichia coli* cultures using silicone-based sorptive media and thermal desorption GC–MS. J Sep Sci. 2018;41(22):4133–41.
53. Malcolm A, Wright S, Syms RR, Moseley RW, O'Prey S, Dash N, et al. A miniature mass spectrometer for liquid chromatography applications. Rapid Commun Mass Spectrom. 2011;25(21):3281–8.
54. Radadia A, Salehi-Khojin A, Masel R, Shannon M. The fabrication of all-silicon micro gas chromatography columns using gold diffusion eutectic bonding. J Micromech Microeng. 2009;20(1):015002.
55. Persaud K, Dodd G. Analysis of discrimination mechanisms in the mammalian olfactory system using a model nose. Nature. 1982;299(5881):352.
56. Lombard GL, Dowell V. Comparison of three reagents for detecting indole production by anaerobic bacteria in microtest systems. J Clin Microbiol. 1983;18(3):609–13.
57. Barsan N, Schweizer-Berberich M, Göpel W. Fundamental and practical aspects in the design of nanoscaled SnO_2 gas sensors: a status report. Fresenius' J Anal Chem. 1999;365(4):287–304.
58. Ryabtsev S, Shaposhnick A, Lukin A, Domashevskaya E. Application of semiconductor gas sensors for medical diagnostics. Sens Actuat B Chem. 1999;59(1):26–9.
59. Nanto H, Minami T, Takata S. Zinc-oxide thin-film ammonia gas sensors with high sensitivity and excellent selectivity. J Appl Phys. 1986;60(2):482–4.
60. Chung W-Y, Sakai G, Shimanoe K, Miura N, Lee D-D, Yamazoe N. Preparation of indium oxide thin film by spin-coating method and its gas-sensing properties. Sens Actuat B Chem. 1998;46(2):139–45.
61. Frank J, Fleischer M, Meixner H. Gas-sensitive electrical properties of pure and doped semiconducting Ga_2O_3 thick films. Sens Actuat B Chem. 1998;48(1–3):318–21.
62. Tamaki J, Naruo C, Yamamoto Y, Matsuoka M. Sensing properties to dilute chlorine gas of indium oxide based thin film sensors prepared by electron beam evaporation. Sens Actuat B Chem. 2002;83(1–3):190–4.
63. Jung S-J, Yanagida H. The characterization of a CuO/ZnO heterocontact-type gas sensor having selectivity for CO gas. Sens Actuat B Chem. 1996;37(1–2):55–60.
64. Devi GS, Manorama S, Rao V. SnO_2/Bi_2O_3: a suitable system for selective carbon monoxide detection. J Electrochem Soc. 1998;145(3):1039–44.
65. Windischmann H, Mark P. A model for the operation of a thin-film SnOx conductance-modulation carbon monoxide sensor. J Electrochem Soc. 1979;126(4):627–33.
66. Martin MA, Santos J, Vasquez H, Agapito J. Study of the interferences of NO_2 and CO in solid state commercial sensors. Sens Actuat B Chem. 1999;58(1):469–73.
67. Tang Z, Fung SK, Wong DT, Chan PC, Sin JK, Cheung PW. An integrated gas sensor based on tin oxide thin-film and improved micro-hotplate. Sens Actuat B Chem. 1998;46(3):174–9.
68. Heilig A, Barsan N, Weimar U, Schweizer-Berberich M, Gardner J, Göpel W. Gas identification by modulating temperatures of SnO_2-based thick film sensors. Sens Actuat B Chem. 1997;43(1–3):45–51.
69. Egashira M, Shimizu Y, Takao Y. Trimethylamine sensor based on semiconductive metal oxides for detection of fish freshness. Sens Actuat B Chem. 1990;1(1–6):108–12.
70. Frietsch M, Zudock F, Goschnick J, Bruns M. CuO catalytic membrane as selectivity trimmer for metal oxide gas sensors. Sens Actuat B Chem. 2000;65(1–3):379–81.
71. Lang A, Fleischer M, Meixner H. Surface modifications of Ga_2O_3 thin film sensors with Rh, Ru and Ir clusters. Sens Actuat B Chem. 2000;66(1–3):80–4.
72. de Lacy CB, Ewen RJ, Ratcliffe NM, Sivanand P. Thick film organic vapour sensors based on binary mixtures of metal oxides. Sens Actuat B Chem. 2003;92(1–2):159–66.
73. Tan O, Zhu W, Yan Q, Kong L. Size effect and gas sensing characteristics of nanocrystalline $xSnO_2$-(1−x) α-Fe_2O_3 ethanol sensors. Sens Actuat B Chem. 2000;65(1–3):361–5.
74. Taurino A, Capone S, Siciliano P, Toccoli T, Boschetti A, Guerini L, et al. Nanostructured TiO_2 thin films prepared by supersonic beams and their application in a sensor array for the discrimination of VOC. Sens Actuat B Chem. 2003;92(3):292–302.
75. Comini E, Faglia G, Sberveglieri G, Li Y, Wlodarski W, Ghantasala M. Sensitivity enhancement towards ethanol and methanol of TiO_2 films doped with Pt and Nb. Sens Actuat B Chem. 2000;64(1–3):169–74.
76. Fang G, Liu Z, Liu C, Yao KL. Room temperature H2S sensing properties and mechanism of CeO_2–SnO_2 sol–gel thin films. Sens Actuat B Chem. 2000;66(1–3):46–8.
77. Devi GS, Manorama S, Rao V. Gas sensitivity of SnO_2/CuO heterocontacts. J Electrochem Soc. 1995;142(8):2754–7.
78. Di Natale C, Davide F, Faglia G, Nelli P. Study of the effect of the sensor operating temperature on SnO_2-based sensor-array performance. Sens Actuat B Chem. 1995;23(2–3):187–91.
79. Tamaki J, Yamada Y, Yamamoto Y, Matsuoka M, Ota I. Sensing properties to dilute hydrogen sulfide of $ZnSb_2O_6$ thick-film prepared by dip-coating method. Sens Actuat B Chem. 2000;66(1–3):70–3.
80. Kimura M. Absolute-humidity sensing independent of the ambient temperature. Sens Actuat A. 1996;55(1):7–11.
81. Satyanarayana L, Reddy CG, Manorama S, Rao V. Liquid-petroleum-gas sensor based on a spinel semiconductor, $ZnGa_2O_4$. Sens Actuat B Chem. 1998;46(1):1–7.

82. Moseley P, Williams D. A selective ammonia sensor. Sens Actuat B Chem. 1990;1(1–6):113–5.
83. Runthala D, Gupta R, Vyas P, Eranna G, Paris R, Schipanski D. A material for room temperature FET sensor to detect ammonia and hydrocarbon gases. Indian J Eng Mater Sci (IJEMS). 2000;7(5–6).
84. Prasad A, Kubinski D, Gouma P. Comparison of sol–gel and ion beam deposited MoO_3 thin film gas sensors for selective ammonia detection. Sens Actuat B Chem. 2003;93(1–3):25–30.
85. Schierbaum K-D. Engineering of oxide surfaces and metal/oxide interfaces for chemical sensors: recent trends. Sens Actuat B Chem. 1995;24(1–3):239–47.
86. Santos J, Serrini P, O'Beirn B, Manes L. A thin film SnO_2 gas sensor selective to ultra-low NO_2 concentrations in air. Sens Actuat B Chem. 1997;43(1–3):154–60.
87. Ishihara T, Sato S, Fukushima T, Takita Y. Capacitive gas sensor of mixed oxide CoO–In_2O_3 to selectively detect nitrogen monoxide. J Electrochem Soc. 1996;143(6):1908–14.
88. Kim S-R, Hong H-K, Kwon CH, Yun DH, Lee K, Sung YK. Ozone sensing properties of In_2O_3-based semiconductor thick films. Sens Actuat B Chem. 2000;66(1–3):59–62.
89. Zhou X, Xu Y, Cao Q, Niu S. Metal-semiconductor ohmic contact of SnO_2-based ceramic gas sensors. Sens Actuat B Chem. 1997;41(1–3):163–7.
90. Saito S, Miyayama M, Koumoto K, Yanagida H. Gas sensing characteristics of porous ZnO and Pt/ZnO ceramics. J Am Ceram Soc. 1985;68(1):40–3.
91. Zhao S, Wei P, Chen S. Enhancement of trimethylamine sensitivity of MOCVD-SnO_2 thin film gas sensor by thorium. Sens Actuat B Chem. 2000;62(2):117–20.
92. Vilanova X, Llobet E, Alcubilla R, Sueiras JE, Correig X. Analysis of the conductance transient in thick-film tin oxide gas sensors. Sens Actuat B Chem. 1996;31(3):175–80.
93. Bhattacharyya P, Basu P, Mondal B, Saha H. A low power MEMS gas sensor based on nanocrystalline ZnO thin films for sensing methane. Microelectron Reliab. 2008;48(11–12):1772–9.
94. Nylander C, Armgarth M, Lundström I. An ammonia detector based on a conducting polymer. In: Seiyama T. editor. Chemical sensors: meeting proceedings. Analytical chemistry symposia series, vol. 17. Elsevier; 1983. p. 203–207.
95. Lu G, Qu L, Shi G. Electrochemical fabrication of neuron-type networks based on crystalline oligopyrene nanosheets. Electrochim Acta. 2005;51(2):340–6.
96. Devaraj H, Travas-Sejdic J, Sharma R, Aydemir N, Williams D, Haemmerle E, et al. Bio-inspired flow sensor from printed PEDOT: PSS micro-hairs. Bioinspir Biomimetics. 2015;10(1):016017.
97. Devaraj H, Sharma R, Haemmerle E, Aw K, editors. A portable & disposable ultra-low velocity flow sensor from bioinspired hair-like microstructures. In: Multidisciplinary digital publishing institute proceedings; 2018.
98. Li B, Sauvé G, Iovu MC, Jeffries-El M, Zhang R, Cooper J, et al. Volatile organic compound detection using nanostructured copolymers. Nano Lett. 2006;6(8):1598–602.
99. Zhang T, Nix MB, Yoo BY, Deshusses MA, Myung NV. Electrochemically functionalized single-walled carbon nanotube gas sensor. Electroanal Int J Devot Fund Pract Aspects Electroanal. 2006;18(12):1153–8.
100. Hernandez SC, Chaudhuri D, Chen W, Myung NV, Mulchandani A. Single polypyrrole nanowire ammonia gas sensor. Electroanal Int J Devot Fund Pract Aspects Electroanal. 1920;2007(19-20):2125–30.
101. Dixit V, Misra S, Sharma B. Carbon monoxide sensitivity of vacuum deposited polyaniline semiconducting thin films. Sens Actuat B Chem. 2005;104(1):90–3.
102. Sadek A, Wlodarski W, Shin K, Kaner RB, Kalantar-Zadeh K. A layered surface acoustic wave gas sensor based on a polyaniline/In_2O_3 nanofibre composite. Nanotechnology. 2006;17(17):4488.
103. Waghuley S, Yenorkar S, Yawale S, Yawale S. Application of chemically synthesized conducting polymer-polypyrrole as a carbon dioxide gas sensor. Sens Actuat B Chem. 2008;128(2):366–73.
104. Misra S, Mathur P, Yadav M, Tiwari M, Garg S, Tripathi P. Preparation and characterization of vacuum deposited semiconducting nanocrystalline polymeric thin film sensors for detection of HCl. Polymer. 2004;45(25):8623–8.
105. Virji S, Fowler JD, Baker CO, Huang J, Kaner RB, Weiller BH. Polyaniline nanofiber composites with metal salts: chemical sensors for hydrogen sulfide. Small. 2005;1(6):624–7.
106. Athawale AA, Bhagwat S, Katre PP. Nanocomposite of Pd-polyaniline as a selective methanol sensor. Sens Actuat B Chem. 2006;114(1):263–70.
107. Xie D, Jiang Y, Pan W, Li D, Wu Z, Li Y. Fabrication and characterization of polyaniline-based gas sensor by ultra-thin film technology. Sens Actuat B Chem. 2002;81(2–3):158–64.
108. Chyla A, Lewandowska A, Soloducho J, Gorecka-Drzazga A, Szablewski M. 4-t-butyl-CuPc-PODT molecular composite material for an effective gas sensor. IEEE Trans Dielectr Electr Insul. 2001;8(3):559–65.
109. Li G, Martinez C, Semancik S. Controlled electrophoretic patterning of polyaniline from a colloidal suspension. J Am Chem Soc. 2005;127(13):4903–9.
110. Kondratowicz B, Narayanaswamy R, Persaud K. An investigation into the use of electrochromic polymers in optical fibre gas sensors. Sens Actuat B Chem. 2001;74(1–3):138–44.
111. Im JS, Kang SC, Lee S-H, Lee Y-S. Improved gas sensing of electrospun carbon fibers based on pore structure, conductivity and surface modification. Carbon. 2010;48(9):2573–81.
112. Leghrib R, Llobet E. Quantitative trace analysis of benzene using an array of plasma-treated metal-decorated carbon nanotubes and fuzzy adaptive resonant theory techniques. Anal Chim Acta. 2011;708(1–2):19–27.
113. Kirkpatrick S. Percolation and conduction. Rev Mod Phys. 1973;45(4):574.
114. Lonergan MC, Severin EJ, Doleman BJ, Beaber SA, Grubbs RH, Lewis NS. Array-based vapor sensing using chemically sensitive, carbon black-polymer resistors. Chem Mater. 1996;8(9):2298–312.
115. Zhang B, Fu R, Zhang M, Dong X, Wang L, Pittman CU Jr. Gas sensitive vapor grown carbon nanofiber/polystyrene sensors. Mater Res Bull. 2006;41(3):553–62.
116. Im JS, Kang SC, Lee S-H, Lee Y-S. Improved gas sensing of electrospun carbon fibers based on pore structure, conductivity and surface modification. Carbon. 2010;48(9):2573–81.
117. Zhang L, Wang X, Zhao Y, Zhu Z, Fong H. Electrospun carbon nano-felt surface-attached with Pd nanoparticles for hydrogen sensing application. Mater Lett. 2012;68:133–6.
118. Lee JS, Kwon OS, Park SJ, Park EY, You SA, Yoon H, et al. Fabrication of ultrafine metal-oxide-decorated carbon nanofibers for DMMP sensor application. ACS Nano. 2011;5(10):7992–8001.
119. Tans SJ, Verschueren AR, Dekker C. Room-temperature transistor based on a single carbon nanotube. Nature. 1998;393(6680):49.
120. Kong J, Franklin NR, Zhou C, Chapline MG, Peng S, Cho K, et al. Nanotube molecular wires as chemical sensors. Science. 2000;287(5453):622–5.
121. Kong J, Chapline MG, Dai H. Functionalized carbon nanotubes for molecular hydrogen sensors. Adv Mater. 2001;13(18):1384–6.
122. Leghrib R, Llobet E. Quantitative trace analysis of benzene using an array of plasma-treated metal-decorated carbon nanotubes and

fuzzy adaptive resonant theory techniques. Anal Chim Acta. 2011;708(1–2):19–27.
123. Schedin F, Geim A, Morozov S, Hill E, Blake P, Katsnelson M, et al. Detection of individual gas molecules adsorbed on graphene. Nat Mater. 2007;6(9):652.
124. Villalpando-Paez F, Romero A, Munoz-Sandoval E, Martınez L, Terrones H, Terrones M. Fabrication of vapor and gas sensors using films of aligned CNx nanotubes. Chem Phys Lett. 2004;386(1–3):137–43.
125. Li W, Geng X, Guo Y, Rong J, Gong Y, Wu L, et al. Reduced graphene oxide electrically contacted graphene sensor for highly sensitive nitric oxide detection. ACS Nano. 2011;5(9):6955–61.
126. Gottardi G, Galli E. Natural zeolites. New York: Springer; 2012.
127. Long JR, Yaghi OM. The pervasive chemistry of metal–organic frameworks. Chem Soc Rev. 2009;38(5):1213–4.
128. O'Keeffe M. Design of MOFs and intellectual content in reticular chemistry: a personal view. Chem Soc Rev. 2009;38(5):1215–7.
129. Perry Iv JJ, Perman JA, Zaworotko MJ. Design and synthesis of metal–organic frameworks using metal–organic polyhedra as supermolecular building blocks. Chem Soc Rev. 2009;38(5):1400–17.
130. James SL. Metal–organic frameworks. Chem Soc Rev. 2003;32(5):276–88.
131. Furukawa H, Cordova KE, O'Keeffe M, Yaghi OM. The chemistry and applications of metal–organic frameworks. Science. 2013;341(6149):1230444.
132. Lu Z-Z, Zhang R, Li Y-Z, Guo Z-J, Zheng H-G. Solvatochromic behavior of a nanotubular metal–organic framework for sensing small molecules. J Am Chem Soc. 2011;133(12):4172–4.
133. Kreno LE, Leong K, Farha OK, Allendorf M, Van Duyne RP, Hupp JT. Metal–organic framework materials as chemical sensors. Chem Rev. 2011;112(2):1105–25.
134. Lee J-H, Houk R, Robinson A, Greathouse J, Thornberg S, Allendorf M, et al., editors. Investigation of microcantilever array with ordered nanoporous coatings for selective chemical detection. In: Micro-and nanotechnology sensors, systems, and applications II. International Society for Optics and Photonics; 2010.
135. Cote AP, Benin AI, Ockwig NW, O'keeffe M, Matzger AJ, Yaghi OM. Porous, crystalline, covalent organic frameworks. Science. 2005;310(5751):1166–70.
136. Ding S-Y, Wang W. Covalent organic frameworks (COFs): from design to applications. Chem Soc Rev. 2013;42(2):548–68.
137. Feng X, Ding X, Jiang D. Covalent organic frameworks. Chem Soc Rev. 2012;41(18):6010–22.
138. Das G, Biswal BP, Kandambeth S, Venkatesh V, Kaur G, Addicoat M, et al. Chemical sensing in two dimensional porous covalent organic nanosheets. Chem Sci. 2015;6(7):3931–9.
139. Li Z, Zhang Y, Xia H, Mu Y, Liu X. A robust and luminescent covalent organic framework as a highly sensitive and selective sensor for the detection of Cu2+ ions. Chem Commun. 2016;52(39):6613–6.
140. Ding S-Y, Dong M, Wang Y-W, Chen Y-T, Wang H-Z, Su C-Y, et al. Thioether-based fluorescent covalent organic framework for selective detection and facile removal of mercury(II). J Am Chem Soc. 2016;138(9):3031–7.
141. Laftah WA, Hashim S, Ibrahim AN. Polymer hydrogels: a review. Polym Plast Technol Eng. 2011;50(14):1475–86.
142. Gerlach G, Guenther M, Suchaneck G, Sorber J, Arndt KF, Richter A, editors. Application of sensitive hydrogels in chemical and pH sensors. In: Macromolecular symposia. Wiley Online Library; 2004.
143. Trinh QT, Gerlach G, Sorber J, Arndt K-F. Hydrogel-based piezoresistive pH sensors: design, simulation and output characteristics. Sens Actuat B Chem. 2006;117(1):17–26.
144. Kojima J, Nakayama Y, Takenaka M, Hashimoto T. Apparatus for measuring time-resolved light scattering profiles from supercritical polymer solutions undergoing phase separation under high pressure. Rev Sci Instrum. 1995;66(8):4066–72.
145. Zguris J, Pishko MV. Nitric oxide sensitive fluorescent poly(ethylene glycol) hydrogel microstructures. Sens Actuat B Chem. 2006;115(1):503–9.
146. Herber S, Olthuis W, Bergveld P, van den Berg A. Exploitation of a pH-sensitive hydrogel disk for CO_2 detection. Sens Actuat B Chem. 2004;103(1–2):284–9.
147. Bai H, Sheng K, Zhang P, Li C, Shi G. Graphene oxide/conducting polymer composite hydrogels. J Mater Chem. 2011;21(46):18653–8.
148. Wu J, Tao K, Zhang J, Guo Y, Miao J, Norford LK. Chemically functionalized 3D graphene hydrogel for high performance gas sensing. J Mater Chem A. 2016;4(21):8130–40.
149. Tuerk C, Gold L. Systematic evolution of ligands by exponential enrichment: RNA ligands to bacteriophage T4 DNA polymerase. Science. 1990;249(4968):505–10.
150. Ellington AD, Szostak JW. In vitro selection of RNA molecules that bind specific ligands. Nature. 1990;346(6287):818.
151. Stoltenburg R, Reinemann C, Strehlitz B. FluMag-SELEX as an advantageous method for DNA aptamer selection. Anal Bioanal Chem. 2005;383(1):83–91.
152. Berezovski M, Musheev M, Drabovich A, Krylov SN. Non-SELEX selection of aptamers. J Am Chem Soc. 2006;128(5):1410–1.
153. Cao Z, Tong R, Mishra A, Xu W, Wong GC, Cheng J, et al. Reversible cell-specific drug delivery with aptamer-functionalized liposomes. Angew Chem Int Ed. 2009;48(35):6494–8.
154. Bagalkot V, Farokhzad OC, Langer R, Jon S. An aptamer–doxorubicin physical conjugate as a novel targeted drug-delivery platform. Angew Chem Int Ed. 2006;45(48):8149–52.
155. Huang YF, Shangguan D, Liu H, Phillips JA, Zhang X, Chen Y, et al. Molecular assembly of an aptamer–drug conjugate for targeted drug delivery to tumor cells. ChemBioChem. 2009;10(5):862–8.
156. Shangguan D, Cao Z, Meng L, Mallikaratchy P, Sefah K, Wang H, et al. Cell-specific aptamer probes for membrane protein elucidation in cancer cells. J Proteome Res. 2008;7(5):2133–9.
157. Wang L, Zhu J, Han L, Jin L, Zhu C, Wang E, et al. Graphene-based aptamer logic gates and their application to multiplex detection. ACS Nano. 2012;6(8):6659–66.
158. He Y, Xing X, Tang H, Pang D. Graphene oxide-based fluorescent biosensor for protein detection via terminal protection of small-molecule-linked DNA. Small. 2013;9(12):2097–101.
159. Sun W, Shi S, Yao T. Graphene oxide–Ru complex for label-free assay of DNA sequence and potassium ions via fluorescence resonance energy transfer. Anal Methods. 2011;3(11):2472–4.
160. Wen Y, Xing F, He S, Song S, Wang L, Long Y, et al. A graphene-based fluorescent nanoprobe for silver(I) ions detection by using graphene oxide and a silver-specific oligonucleotide. Chem Commun. 2010;46(15):2596–8.
161. Zhang JR, Huang WT, Xie WY, Wen T, Luo HQ, Li NB. Highly sensitive, selective, and rapid fluorescence Hg2+ sensor based on DNA duplexes of poly(dT) and graphene oxide. Analyst. 2012;137(14):3300–5.
162. Staii C, Johnson AT, Chen M, Gelperin A. DNA-decorated carbon nanotubes for chemical sensing. Nano Lett. 2005;5(9):1774–8.
163. So HM, Park DW, Jeon EK, Kim YH, Kim BS, Lee CK, et al. Detection and titer estimation of Escherichia coli using aptamer-functionalized single-walled carbon-nanotube field-effect transistors. Small. 2008;4(2):197–201.
164. Lian Y, He F, Wang H, Tong F. A new aptamer/graphene interdigitated gold electrode piezoelectric sensor for rapid and specific detection of *Staphylococcus aureus*. Biosens Bioelectron. 2015;65:314–9.

165. Angioy AM, Desogus A, Barbarossa IT, Anderson P, Hansson BS. Extreme sensitivity in an olfactory system. Chem Senses. 2003;28(4):279–84.
166. Kaupp UB. Olfactory signalling in vertebrates and insects: differences and commonalities. Nat Rev Neurosci. 2010;11(3):188.
167. Montagné N, de Fouchier A, Newcomb RD, Jacquin-Joly E. Advances in the identification and characterization of olfactory receptors in insects. In: Progress in molecular biology and translational science: Elsevier; 2015. p. 55–80.
168. Khadka R, Aydemir N, Carraher C, Hamiaux C, Colbert D, Cheema J, et al. An ultrasensitive electrochemical impedance-based biosensor using insect odorant receptors to detect odorants. Biosens Bioelectron. 2019;126:207–13.
169. Toyokuni S. Genotoxicity and carcinogenicity risk of carbon nanotubes. Adv Drug Deliv Rev. 2013;65(15):2098–110.